

3D Characterization of Smoke Plume Dispersion Using Multi-View Drone Swarm

Nikil Krishnakumar^a, Shashank Sharma^a, Srijan Kumar Pal^a and Jiarong Hong^{b,*1}

^aMinnesota Robotics Institute, St. Anthony Falls Laboratory, University of Minnesota, Minneapolis, Minnesota, United States

^bMechanical Engineering, St. Anthony Falls Laboratory, University of Minnesota, Minneapolis, Minnesota, United States

ARTICLE INFO

Keywords:

Drone Swarm
Smoke Plume Reconstruction
Environmental Monitoring
Plume Dispersion Characterization

ABSTRACT

The study presents an advanced multi-view drone swarm imaging system for three-dimensional characterization of smoke plumes during controlled burns. The system integrates a manager drone and four worker drones equipped with high-resolution cameras and precise GPS modules. These drones operate autonomously in synchronized circular flight paths to capture multi-angle images, which are processed using Neural Radiance Fields (NeRF) to generate high-resolution 3D reconstructions of the plume's temporal evolution. Field tests validated the system's ability to extract key plume characteristics, such as volume dynamics, directional shifts influenced by wind, and the interplay between smoke generation and lofting, with second-level temporal resolution. This innovative system offers high resolution data for refining predictive models of smoke dispersion and optimizing prescribed burn practices. Furthermore, its versatile design enables broader applications, including monitoring industrial emissions, tracking volcanic ash plumes, and studying atmospheric transport phenomena, making it a powerful tool for environmental and climate research.

1. Introduction

Understanding the transport dynamics of atmospheric particles, such as dust, snow, smoke, and sand, is essential due to its significant impact on air quality, climate, and ecological systems across various environmental processes, including wildfires, sandstorms, snowstorms, and volcanic eruptions (Kumar et al., 2011; Kok et al., 2012; Evangelou et al., 2020; Mott et al., 2010; Jaffe et al., 2020; Butwin et al., 2019; Dentoni et al., 2022). This is important for prescribed burns, which are controlled fires used in forest management to enhance ecological health and reduce the risk of wildfires. However, the occurrence of 43 wildfires out of 50,000 prescribed burns in the U.S. between 2012 and 2021 underscores the need for effective smoke management to ensure public safety and minimize adverse effects on air quality (Associated Press, 2024). The challenges in managing these burns highlight a critical gap in our understanding of the dispersion dynamics of particles during these events, which can lead to severe and potentially devastating outcomes (Kalabokidis, 2000; Pereira et al., 2021). Therefore, there is a pressing need for comprehensive research to better predict, manage, and mitigate the risks associated with prescribed burns.

To address these challenges, researchers are developing various simulation tools, such as QUIC-Fire and FIRETEC (Linn et al., 2020, 2002), that aim to model fire and smoke particle behavior. These tools utilize complex inputs, including 3D maps of fuel sources, vegetation structure, topography, moisture content, and wind predictions (Robinson et al., 2023; Mell et al.,

2021; Rowell et al., 2020). Despite these advancements, significant limitations remain. There is a lack of validation that compares the predicted movement of particles with actual plume dispersion, a shortage of dynamic 3D ground truth data on particle dispersion, and difficulties in making accurate predictions in areas where 3D fuel data is unavailable (Linn et al., 2020; Brambilla, 2023). These limitations underscore the ongoing need for field data to validate and improve these models, ensuring more accurate predictions and better management.

However, current field tools for data collection have significant limitations. Remote sensing and Lidar technologies, while valuable, lack the spatial and temporal resolution required to capture the highly dynamic flows of smoke plumes during prescribed burns (Sokolik et al., 2019; Prichard et al., 2019). Moreover, these tools are constrained by their limited mobility, making it difficult to effectively monitor events across varied terrains or in remote and inaccessible areas. The inability to collect such detailed data hinders the development of more accurate and reliable models for managing prescribed burns and predicting smoke dispersion.

To address these challenges, this study aims to develop an autonomous drone swarm equipped with cameras to capture multi-angle images of smoke plumes. This approach will enable the 3D reconstruction of plume dispersal dynamics, allowing for detailed analysis of flow patterns. By deploying a fleet of drones for multi-view imaging, we intend to create a comprehensive 3D ground truth model of specific burn events. This model will provide researchers with critical data for validating simulation predictions and offer essential guidance for hazard response and management.

While there has been no prior work on 3D reconstruction of particle transport using multi-view images from drones, significant advancements have been made in 3D reconstruction techniques with static objects (Schenk, 2005; Goesele

*Corresponding author.

 krish375@umn.edu (N. Krishnakumar); sharm964@umn.edu (S. Sharma); pal00036@umn.edu (S.K. Pal); jhong@umn.edu (J. Hong)

ORCID(s):

¹ORCID: 0000-0001-7860-2181

et al., 2006; Hackl et al., 2018; Schonberger and Frahm, 2016; Mildenhall et al., 2021; Müller et al., 2022). Prominent methods include Structure from Motion (SfM) and Multi-view Stereo (MVS), which reconstructs 3D models from 2D image sequences through feature tracking and photogrammetry, allowing for precise estimation of camera poses and 3D structures (Goesele et al., 2006; Schonberger and Frahm, 2016). Neural Radiance Fields (NeRF) have further pushed the boundaries of scene reconstruction by generating photorealistic views through the optimization of a continuous 5D neural radiance field from sparse input images (Mildenhall et al., 2021; Müller et al., 2022). Building on these advancements, D-NeRF extends this capability to dynamic scenes, capturing non-rigid motion and deformation over time (Pumarola et al., 2021). Additionally, RoDynRF enables dynamic view synthesis from monocular videos, even without known camera poses (Liu et al., 2023). However, reconstructing atmospheric dispersion plumes presents unique challenges. SfM struggles with the featureless nature of plumes (Schonberger and Frahm, 2016), NeRF is primarily designed for static scenes (Mildenhall et al., 2021; Müller et al., 2022), D-NeRF may not perform well with unfamiliar or highly variable scenes (Pumarola et al., 2021), and RoDynRF faces difficulties with the complex dynamics of plumes and demands extensive training times (Liu et al., 2023). These limitations can be effectively addressed using our multi-view drone swarm approach. By deploying multiple drones, we can adaptively capture images of the plume at various scales and positions, tailored to the plume's size and dynamic evolution. With this adaptive imaging strategy, we can fully harness the efficiency (compared to D-NeRF) and accuracy of the NeRF pipeline, generating highly detailed 3D reconstructions for each temporal snapshot. This approach allows us to capture multiple reconstructions over time, facilitating the study of the plume's dispersion change.

The structure of this paper is as follows: Section II details the proposed drone swarm platform for 3D plume characterization, including both the drone hardware and 3D reconstruction method. Section III demonstrates the efficiency of our system through field deployment of our multi-view drone swarm and the follow-up 3D plume reconstruction and plume characterization. Finally, we summarize our findings and discuss their implications and limitations.

2. Methodology

2.1. Overview

As illustrated in [Figure 1](#), our drone swarm system for multi-view imaging comprises two main components: the data acquisition module and the data processing module. The data acquisition module includes a manager drone and four worker drones, which work in a coordinated manner to capture multi-view images of the smoke plume and its evolution over time. These drones are equipped with synchronized imaging systems that allow them to document the plume at different time steps from various angles.

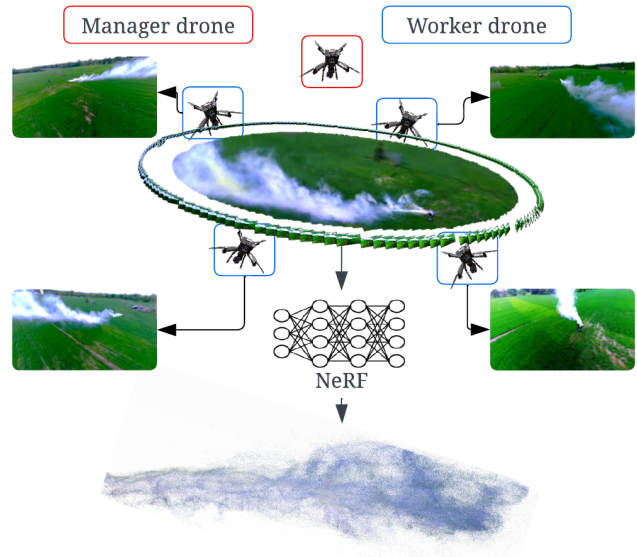


Figure 1: Illustration of the drone swarm system that uses multi-view imaging for 3D smoke plume characterization.

In the data processing module, the captured images from the worker drones are compiled and segregated by segmented time intervals. The images are then fed into the Neural Radiance Fields (NeRF) network, and the output point cloud from this is further processed to remove the background and segment the plume in 3D. This 3D model is used to extract important characteristics of the plume, such as its volume, angle of deviation, and other dynamics of plume dispersion in the atmosphere. The process is repeated for each time segment to provide a comprehensive spatial and temporal characterization of the plume dynamics.

2.2. Data Acquisition Module

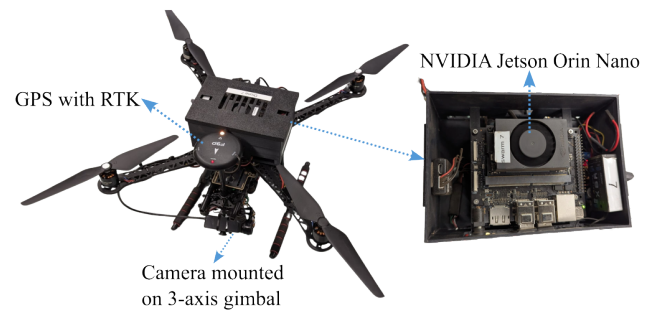


Figure 2: Drone hardware configuration showing the quadcopter with camera mounted on a 3-axis gimbal and GPS with RTK (left), and the NVIDIA Jetson Orin Nano (right).

The drone swarm system consists of a manager drone and four worker drones, built on durable Holybro S500 V2 quadcopter frames. Each drone is equipped with a 12 Megapixel (MP) ArduCam USB-based camera mounted on a 3-axis

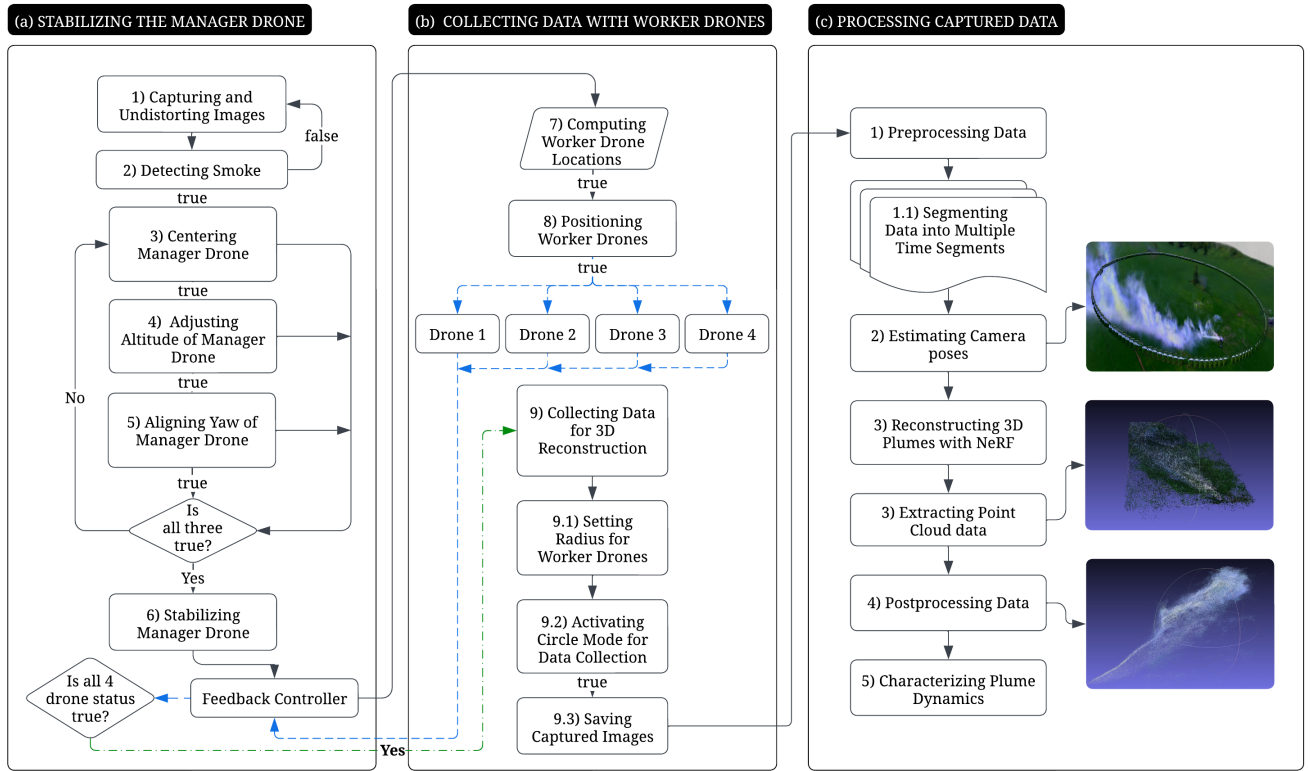


Figure 3: Flowcharts detailing the steps involved in (a) stabilizing the manager drone, (b) collecting data with the worker drone swarm, and (c) processing captured data for 3D plume reconstruction and characterization.

gimbal for smoke detection, image feedback control, and dataset collection to facilitate 3D reconstruction, as shown in Figure 2. The drones are powered by 6000 mAh lithium-polymer batteries and controlled using Holybro Pixhawk 6C flight controllers running ArduPilot. Commands can be transmitted through a 2.4 GHz FrSky RC controller, a 915 MHz telemetry radio via MAVLink, or directly over USB using the NVIDIA Jetson platform. These components are similar to those used in (Bristow et al., 2023).

The manager drone is equipped with an NVIDIA Jetson Orin Nano, while the worker drones use the NVIDIA Jetson Nano. The manager drone has a more powerful computer to handle the higher computational demands of object detection (smoke) and to manage additional navigation controls for both itself and the worker drones. Both types of drones operate with an onboard computer running MAVROS; the manager drone runs ROS Noetic, while the worker drones operate on ROS Melodic. This setup allows the ROS node to access the flight controller's sensor information as topics and facilitates setting parameters for autonomous actions. It supports inter-sensor communication within the drone and drone-to-drone communication for autonomous swarm operations.

To enable coordinated data collection, the drones are interconnected via a robust outdoor Wi-Fi network with a speed of approximately 1775 Mbps, providing stable wireless coverage up to 200-300 m at the 5 GHz band. Additionally, for high-precision positioning, we employ Real-Time

Kinematic (RTK) technology, which provides centimeter-level accuracy by utilizing carrier phase measurements from GNSS signals, achieved through triangulation between the RTK base station, GPS, and satellites. The drones operate based on a swarm control algorithm, depicted in Figure 3, maintaining optimal spacing and coverage around the plume to capture images from multiple perspectives.

1) **Capturing and Undistorting Images:** To ensure accurate 3D reconstruction and image feedback control, camera calibration is performed to determine the camera matrix and distortion coefficients, which are then used to undistort images. In this setup, the manager drone captures images at a resolution of 640 x 480 pixels and processes (segmentation) at a rate of ten fps for realtime feedback, while worker drones use a resolution of 1280 x 720 pixels for better image reconstruction. The full-sensor size of the camera is not used due to its low frame rate and the excessive computational load it would impose on the Jetson Nano.

2) **Detecting Smoke:** The plume detection is conducted using a YOLO-v8(You Only Look Once) (Jocher et al., 2023) segmentation model. This model is trained with top-down views of smoke plumes to accurately detect and segment the plume region.

3) **Centering Manager Drone:** The drone tracks and centers on the plume's centroid obtained from plume segmentation in the previous step by adjusting its position until the centroid is within a specified threshold of the image center. It accomplishes this by publishing velocity commands

(cmd_vel) with twist values for the x and y axes to the drone via MAVROS. These commands move the drone in the direction of the centroid. The process continues until the centroid is aligned with the image center, ensuring accurate tracking.

4) Adjusting Altitude of Manager Drone: The drone adjusts its altitude based on the segmented smoke area, ensuring optimal positioning for effective tracking. If the smoke area exceeds an upper threshold, the drone ascends; conversely, if the smoke area falls below a lower threshold, the drone descends. This process continues until the drone reaches the optimal range, where the smoke area comprises 8% to 12% of the image. This threshold is chosen to ensure that most of the smoke is captured within the frame, while still including a portion of the background. Maintaining this balance helps in accurately positioning the drone for swarm operations, allowing the drones to surround the smoke plume effectively and coordinate the mission.

5) Aligning Yaw of Manager Drone: To align the drone perpendicularly to the flow of the dispersion plume, the covariance of the segmented mask is calculated, resulting in eigenvectors that indicate the plume's flow direction relative to the image. The drone is then yawed perpendicular to the largest eigenvector. Using the drone's current heading, yaw adjustment is calculated and executed to achieve desired orientation.

6) Stabilizing Manager Drone: The three processes are re-initiated repeatedly until all parameters fall within their thresholds. Once these conditions are met, the drone stabilizes and maintains its position, ensuring it is correctly aligned and in the optimal location.

7) Computing Worker Drone Locations: Using the drone's GPS coordinates, altitude, and camera focal length, we calculate the real-world dimensions of the captured image. By applying the haversine formula, we calculate the latitude and longitude of the image's corners, based on the known latitude and longitude of the image center. Using this information, we compute an affine transformation matrix with the least error, that maps each pixel to its corresponding GPS coordinates.

8) Positioning Worker Drones: To precisely localize and position the drones around the plume from four sides, the target locations for each drone are calculated based on data from the manager drone. The manager drone captures a 640 x 480-pixel image, and the two vertical extreme points of this image are identified to maximize coverage of the smoke plume while collecting data. The distance from the center to these vertical extremes is used to determine corresponding horizontal positions, ensuring that all worker drones are equidistant from the center. The positions will adjust with each run based on the size of the plume, as the altitude of the manager drone changes accordingly to accommodate plume size variations. Once these positions are computed, the drones are dispersed to their designated locations at the desired altitude, yawing to face the manager drone for optimal data collection.

9) Collecting Data for 3D Reconstruction: Worker drones hold their positions until each reaches its designated location as assigned by the manager drone. Once in position, a uniform radius is established for all drones, determined by the distance between the manager drone and the worker drones. This ensures all drones are equidistant from the manager and collectively encompass the targeted plume, achieving optimal spatial resolution for 3D plume reconstruction. Upon receiving a command from the manager drone, all drones simultaneously switch to circling mode, maintaining the specified radius while orbiting and capturing plume images. This synchronized movement ensures precise data collection and consistent image quality across the swarm

2.3. Data Processing Module

The data processing module consists of several stages designed to efficiently handle the data captured by the drones, as depicted in the flow chart in [Figure 3c](#).

1) Preprocessing Data: Each drone captures data corresponding to one-quarter of a circular region. When combined, data from all four drones form a complete circle around the plume, representing a single time segment. As the drones continue capturing data, additional circles are generated, each corresponding to a new time segment. To enhance temporal resolution, data overlaps are introduced between two consecutive time segments, effectively creating additional intermediate time segments

2) Estimating Camera Poses: Distinctive images captured by each drone are labeled and the aggregation of this is fed into COLMAP, which employs SIFT feature extraction, exhaustive feature matching, structure-from-motion, and bundle adjustment. This process estimates camera poses for all drones relative to one another, ensuring that independent reconstructions are aligned within a unified coordinate system.

3) Reconstructing 3D Plumes with NeRF: For each time segment, the required camera poses are extracted from the total poses computed by COLMAP. Using the COLMAP camera trajectory and corresponding image data, a NeRF (Neural Radiance Fields) model is trained. During this process, 2D image data is projected into radiance fields, which converge to form a 3D representation. The resulting 3D data outside the defined enclosure region is cropped, and the refined data is exported as point clouds.

4) Post-Processing Data: Background removal is performed using a combination of YOLO-v8 and a Naive Bayes Gaussian model. YOLO-v8 is used to detect and segment smoke plumes in three randomly selected images from the input data. These segmented masks, along with the background RGB data, are then used to train a Naive Bayes Gaussian classifier. The classifier is employed to segment the smoke plumes from the point clouds, effectively removing the background.

5) Characterizing Plume Dynamics: In the final step, the processed 3D model is analyzed to extract crucial plume characteristics, such as spatial extent and expansion angle.

These features are essential for understanding plume dynamics and supporting the development of predictive models for behavior in various atmospheric conditions.

3. System Demonstration

3.1. Field Deployment

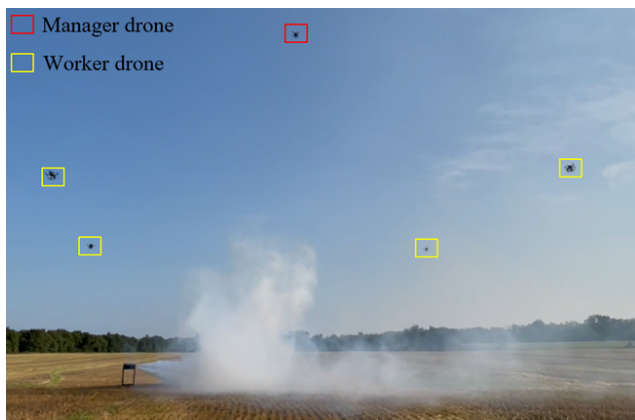


Figure 4: Field deployment setup for data collection, featuring a manager drone positioned above the plume for centralized control and four worker drones encircling the plume to capture multi-angle images for 3D reconstruction.

The field testing was conducted on an agricultural field, as shown in [Figure 4](#). For the testing, smoke plumes were generated using a high-density smoke generator that utilizes a non-harmful smoke fluid composed of high-density fog liquid, food-grade glycerine, and propylene glycol. The generated smoke typically extended up to 40 m in length, with variability depending on the smoke machine's emission intensity. To enhance production, two smoke machines were used: one produced a high volume of smoke that diminished and regenerated cyclically, while the other operated intermittently to optimize overall density. Together, these machines created plumes with widths ranging from one to ten meters and a maximum height of ten meters.

Once the smoke generator and Wi-Fi network were set up, the drones were powered on and connected to the network. We initiate MAVROS nodes in each drone via Secure Socket Shell (SSH), with the manager drone serving as the ROS Master. From the base station, commands were executed to begin operations. The manager drone was launched manually first to process images and relay data to the base station. Upon detecting smoke, the drone was switched to GUIDED mode to autonomously position itself above the plume. Following this, worker drones were launched and set to GUIDED mode to autonomously adjust their positions and optimize coverage based on plume size.

In the experiment, the drones followed circular paths with an average radius of 21 m around the plume. Each drone completed a full circle in approximately 32 s, recording data at eight fps. Equipped with 6000 mAh, 4S batteries, each drone could perform up to five complete circles before experiencing performance degradation, such as altitude drops

due to reduced thrust voltage. At this proof-of-concept stage, the system provided two minutes and 20 s of stable flight time, allowing for five full data collection circuits. All data were recorded onboard for post-flight analysis.

3.2. 3D Plume Reconstruction

In this study, we applied Neural Radiance Fields (NeRF) to reconstruct the 3D dynamics of a smoke plume over two minutes and 20 s recording interval, during which each drone completed five revolutions around the plume. The reconstruction was based on images captured by four drones, each circling the plume at quarter-circle intervals. Each drone required eight seconds to complete a quarter-circle, and because all drones operated synchronously, the combined data provided a full-circle dataset every eight seconds. During each quarter-circle, a drone captured 65 images, resulting in a total of 260 images per full revolution. These images were then processed to reconstruct the plume in 20 distinct time segments, with each segment covering approximately eight seconds of plume dynamics.

To enhance temporal resolution and capture smoother plume dynamics, we introduced overlaps of 25%, 50%, and 75% between time segments, generating three additional reconstructions between each pair of segments. This approach resulted in a total of 77 reconstructed time segments, providing a finer temporal resolution of 1.75 s. This adjustment enabled a more detailed and continuous observation of plume behavior over time.

The 3D reconstruction was performed using a high-performance computing system equipped with a 13th Gen Intel Core i7-13700K CPU, 64 GB of RAM, and an NVIDIA RTX 5000 Ada GPU with 32 GB of memory. The computational time for each 8-second segment was approximately 10 minutes. The process for reconstructing and saving filtered point clouds from segregated data has been fully automated, ensuring efficiency and consistency in data handling.

As shown in [Figure 5](#), the reconstructed models capture significant changes in plume dynamics over the recording period. Snapshots reveal the plume's variations in volume, direction, and shape. Early in the sampling period, the plume exhibits an average volume and elevation, while later stages show greater dispersion, distinct directional deviations, and reduced density. Key stages include initial growth and ascent, lateral dispersion under wind influence, and eventual dissipation with diminished volume and height. The reconstructed models reveal critical changes in the plume's evolution over time, showcasing its growth, directional shifts, and eventual dissipation. These dynamic reconstructions lay the groundwork for quantitative analysis of plume characteristics, discussed in the following section.

3.3. Quantitative Characterization of Plume Dynamics

This section highlights the capability of our drone swarm-based 3D reconstruction system to quantitatively analyze essential plume parameters for controlled burns. From the reconstructed 3D models, we extracted critical

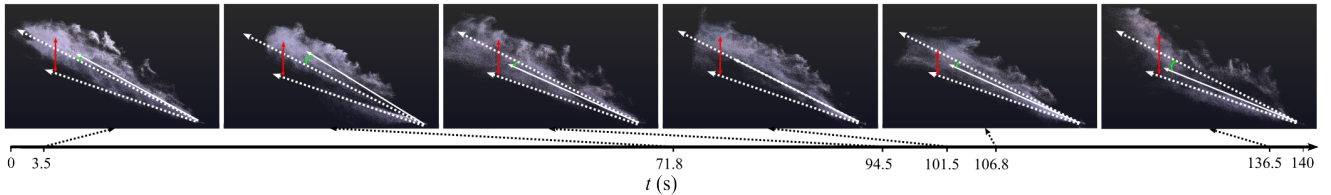


Figure 5: Snapshots of the 3D reconstructed plume showing variations in volume, direction, and shape over the 140 s sampling period. Major dotted lines indicate reference lines for the angle of deviation, with the green-highlighted angle between the major dotted line and the white solid line representing the angle of deviation. Minor dotted lines serve as reference lines for average height, while the vertical red line highlights the average height.

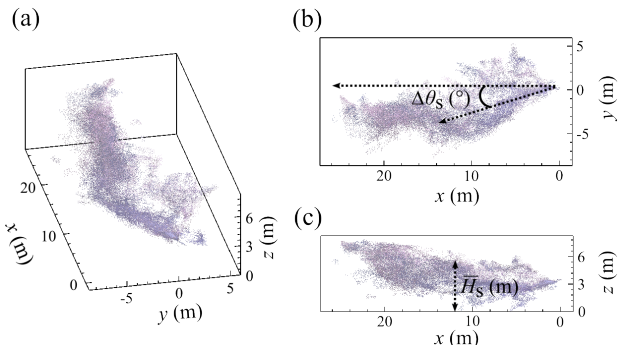


Figure 6: Quantitative analysis of reconstructed plume dynamics: (a) Volume trends over time, showing cyclic behavior, (b) Side view (x - z plane) illustrating variations in average plume height, and (c) Top view (x - y plane) depicting angle of deviation and directional changes.

metrics: total plume volume V_s , angle of deviation (AOD) $\Delta\theta_s$, and average plume height \bar{H}_s . Researchers modeling plumes have shown significant interest in studying changes in elevation and volume to better understand plume lifecycles (Raznjevic, 2023; Cao et al., 2021). AOD has been particularly critical in the development of tools like QUIC-Fire, as it captures the influence of wind on particle transport and fire behavior (Robinson et al., 2023). Guided by these findings, we incorporated the extraction of these parameters into our 3D reconstruction models to enhance the analysis of smoke dynamics. These metrics provide valuable insights into plume behavior, including growth, transport direction, and lofting, which are crucial for applications such as prescribed burn management and forest fire research.

To calculate these critical parameters of plume dynamics, specific methodologies were applied to the reconstructed 3D data, as illustrated in Figure 6. The V_s was estimated using the Convex Hull approach, which encloses the plume's data points within the smallest convex shape, providing a practical, though approximate, measure of its spatial boundaries. This method allowed us to plot the plume's volume changes over time. The $\Delta\theta_s$, reflecting the influence of wind on plume direction, was determined by projecting the plume onto a horizontal plane and calculating the average x and y coordinates. A vector connecting these coordinates to the plume's origin was used to compute the angle between this

vector and a reference line parallel to the x -axis, representing the plume's average direction. Lastly, the \bar{H}_s of the plume was analyzed by calculating the mean elevation of all points in the cloud and plotting it against time.

To ensure these computed parameters were scaled to real-world dimensions, we utilized the known diameter of the drone trajectories. The NeRF model reconstructs data based on trajectory and pose estimations derived from COLMAP, which adheres to a unified coordinate system. By applying the known real-world diameter of the drone paths as a scaling factor, the reconstructed data could be converted into real-world measurement units, enabling physical interpretation of the plume volume, AOD, and height.

Based on the calculation methods described above, each parameter (V_s , $\Delta\theta_s$, \bar{H}_s) was computed, and the results are presented in Figure 7. The trends are analyzed as follows:

1) Volume Change Analysis: As shown in Figure 7a, the plume's volume exhibits a cyclic pattern over time, with distinct peaks and troughs corresponding to periods of smoke generation and diminishment. These fluctuations align with the operation of the smoke machines, where active emissions produce large, dense plumes, and intervals of reduced output result in smaller, more dispersed plumes. This cyclic behavior reflects the temporal dynamics of the plume, driven by the smoke machine's operational cycles. Validation using drone-captured images confirms this pattern, showcasing high-volume plumes during active phases and diminished plumes during quieter intervals. The alignment between these visual observations and the plotted data supports the accuracy of the extracted volume measurements.

2) AOD Analysis: The angle of deviation, as shown in Figure 7b, captures directional shifts in the plume's trajectory under the influence of wind. During steady wind conditions, deviations are minimal, with a typical range of $\pm 10^\circ$. However, when the second smoke machine activates, the plume intensity increases, resulting in higher velocity and longer travel distances. In these cases, the wind's influence becomes more pronounced, causing distinct peaks in the AOD plot. Visual validation highlights this behavior, with the plume initially remaining straight due to the machine's propulsion, then displaying a turning effect as dispersion increases. The visuals also include a reference line that clearly illustrates deviations from the plume's average direction,

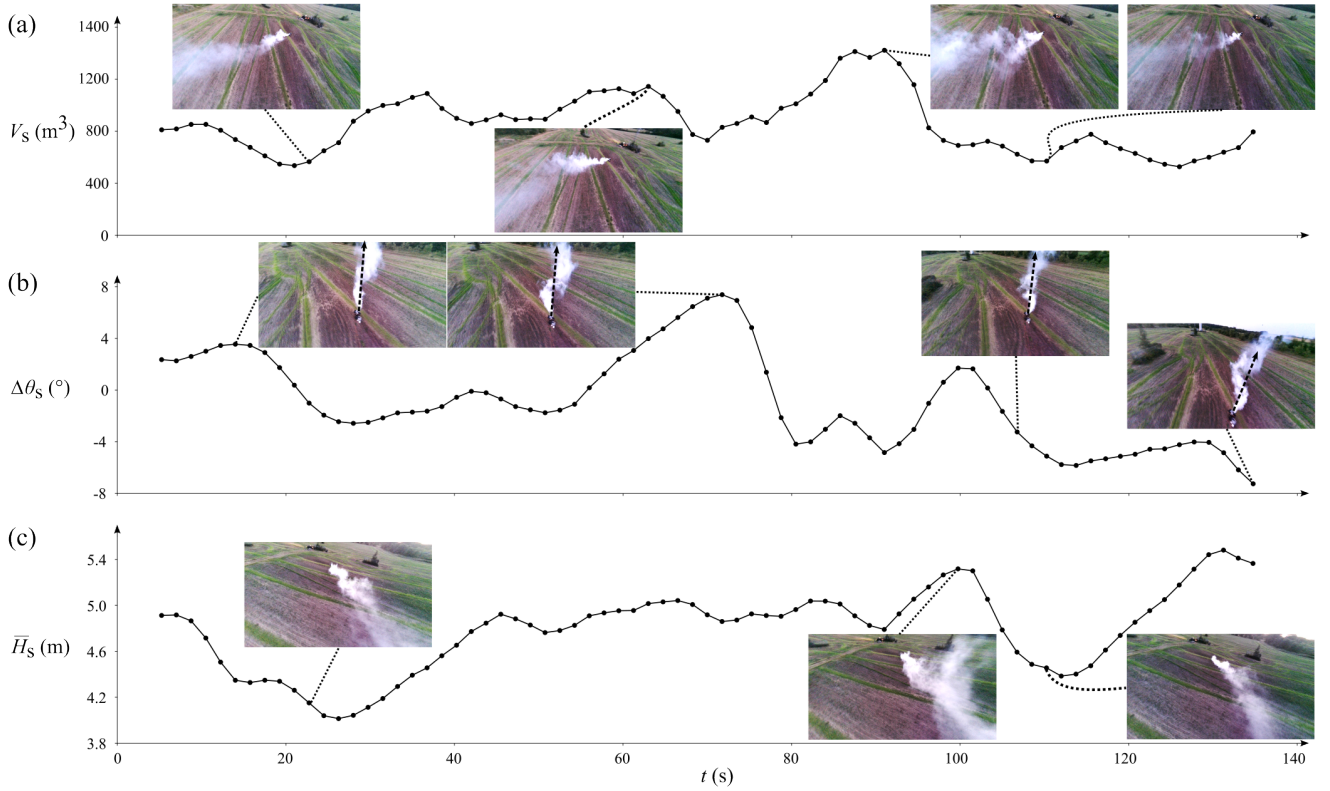


Figure 7: Temporal trends in plume characteristics derived from 3D reconstructions, showing the variation in (a) volume (V_s), (b) angle of deviation ($\Delta\theta_s$), and (c) average height (\bar{H}_s), validated with visual data from individual drone recordings.

emphasizing the transition from machine-driven to wind-driven behavior.

3) Average Height Analysis: The trends in average height, depicted in Figure 7c, closely follow the volume pattern in Figure 7a for most of the recording period. During active smoke generation, the plume achieves higher elevations, especially when wind direction aligns with the plume's flow. Conversely, reduced emissions result in lower plume heights, with the smoke dispersing rapidly at the far end due to wind effects. Notable exceptions occur when \bar{H}_s remains relatively high despite low V_s , which is attributed to narrower plume widths maintaining lofting while reducing overall volume. Validation with drone-captured visuals further supports these observations, illustrating the interplay between smoke generation, vertical expansion, and wind-driven dissipation.

Overall, the deployment of the swarm-based 3D reconstruction system effectively captured and characterized the dynamic nature of smoke plumes, highlighting critical behaviors such as cyclic volume variations, wind-driven directional changes, and the intricate interplay between smoke generation and lofting.

3.4. Conclusion and Discussion

This study presented a novel drone swarm system for 3D reconstruction of dynamic smoke plumes, combining multi-view imaging with Neural Radiance Fields (NeRF) to

achieve high-resolution temporal and spatial plume characterization. The system comprises one manager drone and four worker drones working in a coordinated fashion, with each drone equipped with high-resolution cameras, RTK-enabled GPS for precise positioning, and onboard processing units. Field deployment demonstrated the system's effectiveness in capturing dynamic plume characteristics such as cyclic volume variations, wind-driven directional shifts, and the interplay between smoke generation and lofting. The system reconstructed 77 time segments over a two minute and 20 s interval with a temporal resolution of 1.75 s, yielding detailed quantitative data on plume volume, angle of deviation, and average height. These results validate its precision in analyzing highly dynamic and complex plume dispersal patterns.

The findings underscore the system's transformative potential for prescribed burn control and forest fire research. By providing accurate, dynamic 3D reconstructions, this technology bridges critical gaps in field data required for validating predictive models such as QUIC-Fire and FIRETEC. These capabilities underscore the system's potential to provide precise quantitative insights essential for advancing prescribed burn control strategies and enhancing forest fire research. By enabling detailed visualization and analysis of plume dynamics, this tool demonstrates its capacity to support data-driven decision-making for effective smoke and fire management. Beyond prescribed burns, the system's

versatility extends to other environmental monitoring applications, such as tracking industrial emissions, volcanic ash plumes, and atmospheric particle transport (Butwin et al., 2019; Cao et al., 2021). These advancements have profound implications for improving environmental resilience, disaster response, and air quality management.

Despite its promising capabilities, the current system has limitations. The reliance on fixed circular flight paths restricts adaptability to irregular plume geometries, necessitating waypoint-based or adaptive navigation strategies for more complex scenarios (Tankasala et al., 2022). Using drone sensors to estimate camera poses directly, instead of relying on COLMAP, can significantly reduce computation time. Computational demands for NeRF-based reconstruction pose challenges for real-time applications, requiring optimization through advanced techniques like Dynamic NeRF or instant NGP (Müller et al., 2022; Pumarola et al., 2021). Additionally, the system's current focus on visual data could benefit from the integration of thermal imaging and chemical sensors to capture plume temperature and composition, further expanding its utility (Asadzadeh et al., 2022; Burgués and Marco, 2020). Future work will address these challenges by enhancing drone autonomy, improving computational efficiency, and incorporating multi-modal sensing to create a more robust and versatile plume characterization platform.

Acknowledgements

This work was supported by the NSF Major Research Instrumentation program (NSF- MRI-2018658), which provided crucial funding for the development and deployment of the autonomous drone system for smoke plume characterization. We would also like to extend our gratitude to Sujeendra Ramesh, Sri Ganesh Lalit Aditya Divakarla, and Rammesh Adhav Saravanan for their invaluable assistance during the initial phase of the work.

Declaration of generative AI and AI-assisted technologies in the writing process

During the preparation of this work, the author(s) used ChatGPT for assisting in refining content in this manuscript. After using this tool, the author(s) reviewed and edited the content as needed and take full responsibility for the content of the publication.

References

- Asadzadeh, S., de Oliveira, W.J., de Souza Filho, C.R., 2022. Uav-based remote sensing for the petroleum industry and environmental monitoring: State-of-the-art and perspectives. *Journal of Petroleum Science and Engineering* 208, 109633.
- Associated Press, 2024. Review of prescribed fires finds gaps in key areas as us forest service looks to improve safety. URL: <https://www.voanews.com/a/review-of-prescribed-fires-finds-gaps-in-key-areas-as-us-forest-service-looks-to-improve-safety-/7689105.html>.
- Brambilla, S., 2023. Validation of quic-fire smoke plume dispersion modeling for complex wildland fires. URL: <https://serdp-estcp.mil/projects/details/734feebdb8f7-46ce-b18b-92e7853cbba5/validation-of-quic-fire-smoke-plume-dispersion-modeling-for-complex-wildland-fires.html>.
- Bristow, N.R., Pardoe, N., Hong, J., 2023. Atmospheric aerosol diagnostics with uav-based holographic imaging and computer vision. *IEEE Robotics and Automation Letters*.
- Burgués, J., Marco, S., 2020. Environmental chemical sensing using small drones: A review. *Science of the total environment* 748, 141172.
- Butwin, M.K., von Löwisch, S., Pfeffer, M.A., Thorsteinsson, T., 2019. The effects of volcanic eruptions on the frequency of particulate matter suspension events in iceland. *Journal of Aerosol Science* 128, 99–113.
- Cao, Z., Bursik, M., Yang, Q., Patra, A., 2021. Simulating the transport and dispersal of volcanic ash clouds with initial conditions created by a 3d plume model. *Frontiers in Earth Science* 9, 704797.
- Dentoni, V., Grosso, B., Pinna, F., Lai, A., Bouarour, O., 2022. Emission of fine dust from open storage of industrial materials exposed to wind erosion. *Atmosphere* 13, 320.
- Evangelou, N., Grythe, H., Klimont, Z., Heyes, C., Eckhardt, S., Lopez-Aparicio, S., Stohl, A., 2020. Atmospheric transport is a major pathway of microplastics to remote regions. *Nature communications* 11, 3381.
- Goesele, M., Curless, B., Seitz, S.M., 2006. Multi-view stereo revisited, in: 2006 IEEE Computer Society Conference on Computer Vision and Pattern Recognition (CVPR'06), IEEE. pp. 2402–2409.
- Hackl, J., Adey, B.T., Woźniak, M., Schümperlin, O., 2018. Use of unmanned aerial vehicle photogrammetry to obtain topographical information to improve bridge risk assessment. *Journal of infrastructure systems* 24, 04017041.
- Jaffe, D.A., O'Neill, S.M., Larkin, N.K., Holder, A.L., Peterson, D.L., Halofsky, J.E., Rappold, A.G., 2020. Wildfire and prescribed burning impacts on air quality in the united states. *Journal of the Air & Waste Management Association* 70, 583–615.
- Jocher, G., Chaurasia, A., Qiu, J., 2023. Ultralytics yolo (version 8.0.0). URL: <https://github.com/ultralytics/ultralytics>.
- Kalabokidis, K.D., 2000. Effects of wildfire suppression chemicals on people and the environment—a review. *Global Nest: The International Journal* 2, 129–137.
- Kok, J.F., Parteli, E.J., Michaels, T.I., Karam, D.B., 2012. The physics of wind-blown sand and dust. *Reports on progress in Physics* 75, 106901.
- Kumar, P., Ketzel, M., Vardoulakis, S., Pirjola, L., Britter, R., 2011. Dynamics and dispersion modelling of nanoparticles from road traffic in the urban atmospheric environment—a review. *Journal of Aerosol Science* 42, 580–603.
- Linn, R., Reisner, J., Colman, J.J., Winterkamp, J., 2002. Studying wildfire behavior using firetec. *International journal of wildland fire* 11, 233–246.
- Linn, R.R., Goodrick, S.L., Brambilla, S., Brown, M.J., Middleton, R.S., O'Brien, J.J., Hiers, J.K., 2020. Quic-fire: A fast-running simulation tool for prescribed fire planning. *Environmental Modelling & Software* 125, 104616.
- Liu, Y.L., Gao, C., Meuleman, A., Tseng, H.Y., Saraf, A., Kim, C., Chuang, Y.Y., Kopf, J., Huang, J.B., 2023. Robust dynamic radiance fields, in: Proceedings of the IEEE/CVF Conference on Computer Vision and Pattern Recognition, pp. 13–23.
- Mell, W., Bova, A., Milac, T., 2021. Physics-based modeling of fire behavior and smoke plume development, how much is enough? .
- Mildenhall, B., Srinivasan, P.P., Tancik, M., Barron, J.T., Ramamoorthi, R., Ng, R., 2021. Nerf: Representing scenes as neural radiance fields for view synthesis. *Communications of the ACM* 65, 99–106.
- Mott, R., Schirmer, M., Bavay, M., Grünewald, T., Lehning, M., 2010. Understanding snow-transport processes shaping the mountain snow-cover. *The Cryosphere* 4, 545–559.
- Müller, T., Evans, A., Schied, C., Keller, A., 2022. Instant neural graphics primitives with a multiresolution hash encoding. *ACM transactions on graphics (TOG)* 41, 1–15.
- Pereira, P., Bogunovic, I., Zhao, W., Barcelo, D., 2021. Short-term effect of wildfires and prescribed fires on ecosystem services. *Current Opinion in Environmental Science & Health* 22, 100266.
- Prichard, S., Larkin, N.S., Ottmar, R., French, N.H., Baker, K., Brown, T., Clements, C., Dickinson, M., Hudak, A., Kochanski, A., et al., 2019.

- The fire and smoke model evaluation experiment—a plan for integrated, large fire–atmosphere field campaigns. *Atmosphere* 10, 66.
- Pumarola, A., Corona, E., Pons-Moll, G., Moreno-Noguer, F., 2021. D-nerf: Neural radiance fields for dynamic scenes, in: Proceedings of the IEEE/CVF Conference on Computer Vision and Pattern Recognition, pp. 10318–10327.
- Raznjevic, A., 2023. High-resolution modelling of plume dispersion. Ph.D. thesis. Wageningen University and Research.
- Robinson, D., Brambilla, S., Brown, M.J., Conry, P., Quaife, B., Linn, R.R., 2023. Quic-urb and quic-fire extension to complex terrain: Development of a terrain-following coordinate system. *Environmental Modelling & Software* 159, 105579.
- Rowell, E., Loudermilk, E.L., Hawley, C., Pokswinski, S., Seielstad, C., Queen, L., O'Brien, J.J., Hudak, A.T., Goodrick, S., Hiers, J.K., 2020. Coupling terrestrial laser scanning with 3d fuel biomass sampling for advancing wildland fuels characterization. *Forest Ecology and Management* 462, 117945.
- Schenk, T., 2005. Introduction to photogrammetry. The Ohio State University, Columbus 106, 1.
- Schonberger, J.L., Frahm, J.M., 2016. Structure-from-motion revisited, in: Proceedings of the IEEE conference on computer vision and pattern recognition, pp. 4104–4113.
- Sokolik, I., Soja, A., DeMott, P., Winker, D., 2019. Progress and challenges in quantifying wildfire smoke emissions, their properties, transport, and atmospheric impacts. *Journal of Geophysical Research: Atmospheres* 124, 13005–13025.
- Tankasala, S., Pehlivanturk, C., Bakolas, E., Pryor, M., 2022. Smooth time optimal trajectory generation for drones. arXiv preprint arXiv:2202.09392 .